Lunar Laser Ranging: A Continuing Legacy of the Apollo Program

J. O. Dickey, P. L. Bender, J. E. Faller, X X Newhall, R. L. Ricklefs, J. G. Ries, P. J. Shelus, C. Veillet, A. L. Whipple, J. R. Wiant, J. G. Williams, C. F. Yoder

On 21 July 1969, during the first manned lunar mission, Apollo 11, the first retroreflector array was placed on the moon, enabling highly accurate measurements of the Earth-moon separation by means of laser ranging. Lunar laser ranging (LLR) turns the Earth-moon system into a laboratory for a broad range of investigations, including astronomy, lunar science, gravitational physics, geodesy, and geodynamics. Contributions from LLR include the three-orders-of-magnitude improvement in accuracy in the lunar ephemeris, a several-orders-of-magnitude improvement in the measurement of the variations in the moon's rotation, and the verification of the principle of equivalence for massive bodies with unprecedented accuracy. Lunar laser ranging analysis has provided measurements of the Earth's precession, the moon's tidal acceleration, and lunar rotational dissipation. These scientific results, current technological developments, and prospects for the future are discussed here.

It has been a quarter of a century since the first manned lunar landing by the Apollo 11 astronauts. Included on that mission and the later Apollo 14 and 15 flights were corner-cube retroreflector arrays (Fig. 1A) that permit accurate laser measurement of the Earth-moon separation. The locations of the three Apollo arrays plus one French-built array still operating on the Soviet roving vehicle Lunakhod 2 (Fig. 1B) provide a favorable geometry for studying the rotations of the moon and for separating these rotations from lunar orbital motion and geodynamic effects (Table 1). Unlike the other Apollo scientific experiments, these retroreflector arrays require no power and are still operating normally after 25 years. Accounts of the initial planning stages and early days of the experiment are archived in (*1*). Lunar laser ranging has proven to be a valuable multidisciplinary tool; results in many areas are summarized and reviewed in (*2–7*).

Data Characteristics and Technology Development

Lunar laser ranging consists of measuring the round-trip travel time and thus the separation between transmitter and reflector. Changes of the round-trip travel time contain a wealth of information about the Earth-moon system. The range data have a rich frequency spectrum due to many effects such as the sun's strong influence on the lunar orbit.

Ranging to the moon is technically challenging. An outgoing pulse of laser light transmitted from a collimating telescope with a beam divergence of 3 to 4 s of arc, consistent with atmospheric seeing, spreads to an area approximately 7 km in diameter on the lunar surface. Backscattering from the lunar surface produces a weak, though marginally detectable, signal with a time width characteristic of local lunar topography. Consequently, range measurements to a given target area can vary by the order of a kilometer, which limits their accuracy and applications.

Retroreflector arrays provide optical points on the moon toward which one can fire a laser pulse and receive back a localized and recognizable signal. Ranging accuracies on the order of a centimeter are immediately possible if one has sufficiently short laser pulse lengths with high power. Today, accuracy on the scale of a few centimeters for normal points [compressed data obtained from returns over periods of 10 to 45 min (*8*)] is being obtained routinely.

The design of the Apollo and Lunakhod retroreflector arrays is straightforward. Each corner cube reflects incident light back to its point of origin. The Apollo arrays consist of 100 (Apollo 11 and 14) or 300 (Apollo 15) 3.8-cm-diameter corner cubes mounted in an aluminum panel. The Soviet-French Lunakhod arrays consist of a smaller number (14) of larger, in this case triangularly faced, corner cubes 11 cm on an edge. Although they are subject to thermal distortion during the lunar day because of their greater size, these arrays give approximately the same lunar-night return signal strength as the Apollo arrays.

The arrays intercept only 10^{-9} of the area of the impinging light beam. The angular spread of the returning pulse is set by diffraction, polarization properties, and irregularities of the arrays's individual corner cubes. In the case of the 3.8-cm-diameter Apollo corner cube, the spread is approximately 10 s of arc. Thus, the diameter of the spot produced on the Earth is approximately 20 km. A 1-m-diameter receiving telescope would collect only 2×10^{-9} of the returning photons. A variety of practical matters, such as quantum efficiency, mirror reflectance, optical performance under thermal stress, and velocity aberration (which slightly shifts the center of the returning beam from the location of the transmitting and receiving telescope), make the product of the transmitting, lunar retroreflecting, and receiving efficiencies considerably less than unity. The overall signal loss of approximately 10^{-21} puts a premium on the detailed design of ground stations to minimize their losses. Because 3 J of light, the most energy that one can currently

J. O. Dickey, X X Newhall, J. G. Williams, and C. F. Yoder are at the Jet Propulsion Laboratory, California Institute of Technology, 4800 Oak Grove Drive, Pasadena, CA 91109, USA. P. L. Bender and J. E. Faller are at the Joint Institute for Laboratory Astrophysics, University of Colorado, and National Institute of Standards and Technology, Boulder, CO 80309–0440, USA. R. L. Ricklefs, J. G. Ries, P. J. Shelus, and A. L. Whipple are at the University of Texas–Austin, McDonald Laser Ranging Operations, McDonald Observatory/Astronomy, Austin, TX 78712–1083, USA. J. R. Wiant is at the McDonald Observatory, Fort Davis, TX 79734, USA. C. Veillet is at OCA/CERGA, Avenue Copernic, Grasse F-06130, France.

Table 1. Distribution of LLR Data.

Observatories	Reflector array				Total number of normal points
	Apollo 11	Apollo 14	Apollo 15	Lunakhod 2	
McDonald Observatory 2.7 m (Texas)	468	495	2356	132	3451
MLRS	24	36	607	5	672
Haleakala (Maui, HI)	20	23	633	18	694
CERGA (Grasse, France)	324	339	2699	197	3559

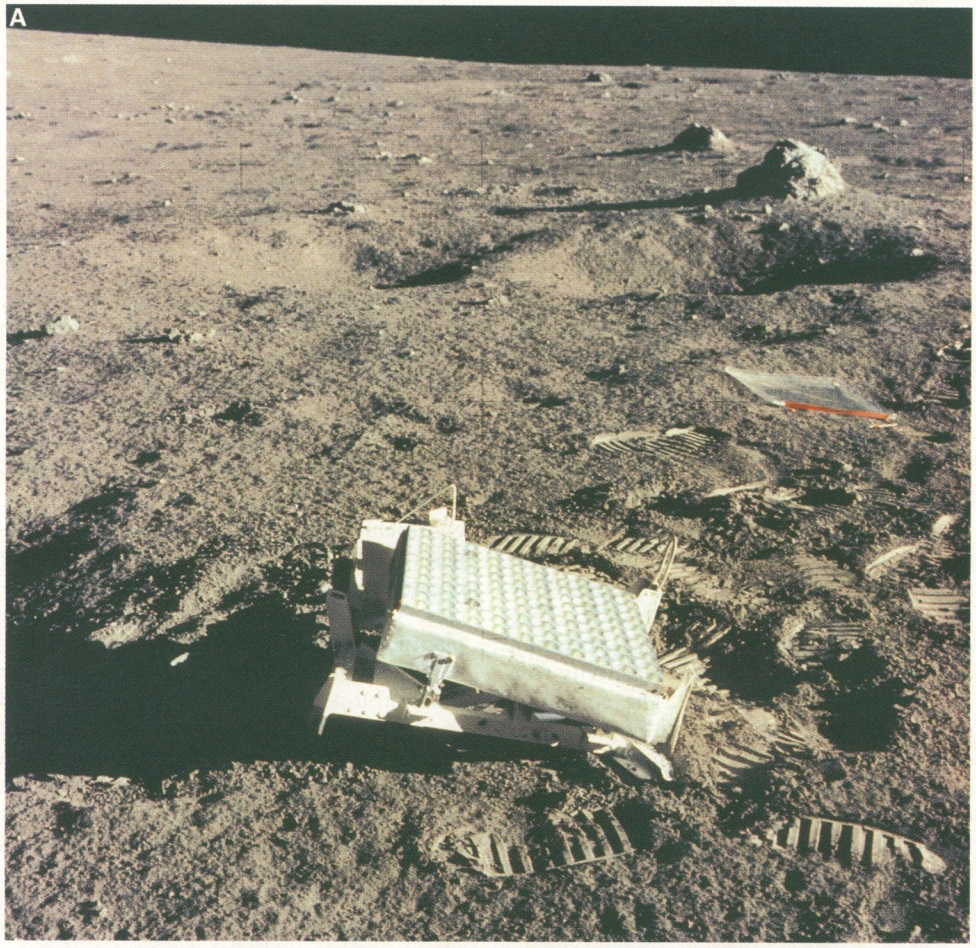

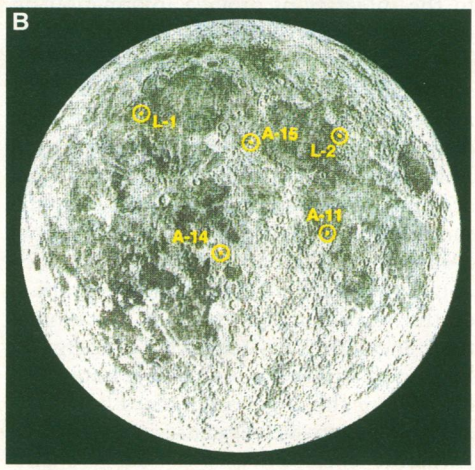

Fig. 1. (**A**) Photograph of a retroreflector array of Apollo 14 on the lunar surface. (**B**) Geographical distribution of the retroreflector arrays on the lunar surface. The labels A-11, A-14, and A-15 denote the Apollo 11, 14, and 15 sites, respectively, whereas L-1 and L-2 indicate the Lunakhod 1 and 2 locations (no returns are available from Lunakhod 1).

transmit per second, contains 10^{19} photons, single-photon detection is a necessity.

At present, there are only a few LLR stations operating, and only one of these is fully dedicated to lunar ranging. The other stations are shared lunar and artificial-satellite ranging facilities. At the time of the Apollo 11 landing, laser ranging was initiated at McDonald Observatory near Fort Davis, Texas, where lunar ranging (shared with artificial-satellite ranging) continues. Preliminary ranging also took place at the Lick Observatory in California where the first returns from the moon were detected (9).

During the first 15 years after the emplacement of the initial retroreflector package on the lunar surface, the McDonald Observatory was the only facility that routinely ranged to the moon. In the late 1960s, the new 2.7-m telescope had just become operational at McDonald, and a commitment to use this instrument in a long-term program of LLR was made. Time-sharing with the observatory's regular astronomical program, McDonald laser operations maintained routine activities for more than 15 years. There were nominally three 45-min observing sessions per day, when the moon was 3 hours east of, on, and 3 hours west of the meridian, some 21 days per lunation (*10*). The data can naturally be divided into three time spans, on the basis of their accuracies (Fig. 2). The early 1970s saw LLR data accuracies at the 25-cm level. Improvements in the 2.7-m LLR timing system reduced measurement to the 15-cm level by the mid-1970s. When the transition was

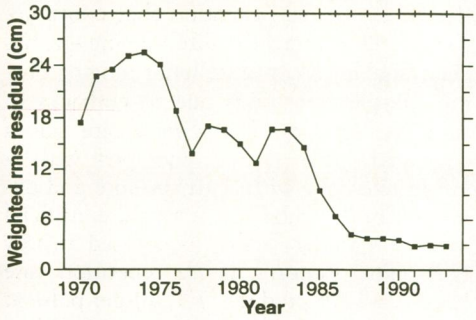

Fig. 2. Histogram of the weighted root-mean-square (rms) post-fit residual (observed minus model) as a function of time.

made in the mid-1980s to the McDonald Laser Ranging System (MLRS) LLR system, accuracies were further improved to the 2- to 3-cm level. Despite this order-of-magnitude improvement in accuracy, the early data are still important in the separation of effects with long characteristic time scales, notably precession, nutation, relativistic geodetic precession, tidal acceleration, the primary lunar oblateness term (J_2), and the relative orientation of the planes of the Earth's equator, the lunar orbit, and the ecliptic.

The 2.7-m McDonald laser ranging system was decommissioned in 1985 and was superseded by a dedicated 0.76-m ranging system, the MLRS, capable of ranging to artificial satellites as well as to the moon (*11*). The present incarnation of the MLRS is constructed around a frequency-doubled, 120-mJ per pulse, 200-ps pulse length (full width at half maximum), neodymium–yttrium-aluminum-garnet (Nd-YAG) laser firing 10 times per second. It has an internal calibration system, and the precision of its epoch timing system is approximately 25 ps. This station now produces LLR data approaching 1-cm normal-point precision (*11*). However, the accuracy is still limited to 2 to 3 cm. In spite of its reduced aperture, which results in fewer data than the 2.7-m telescope could have produced, the shorter laser pulse length has led to a fourfold improvement in the accuracy of the MLRS ranges, providing stronger data than those from the 2.7-m system despite the reduced volume. A number of strategies are being pursued to produce significantly higher volumes of LLR data and further increases in accuracy, including increased station computing, offset guiding and tracking, and improved timing systems.

During the past 8 years, successful ranging has been carried out by a French station [Centre d'Etudes et de Recherche en Geodynamique et Astronomie (CERGA)] at Grasse, located at a 1220-m elevation 20 km north of Cannes with a 1.5-m dedicated LLR telescope, and, until recently, by a second U.S. artificial satellite and lunar ranging station on Maui, Hawaii. Although strong lunar returns were often received by

the latter station—a station that continues to perform artificial satellite ranging—it has been unable to continue lunar ranging during the past few years due to cutbacks in available support. The Grasse site has a dedicated lunar station equipped with a 1.5-m telescope with both absolute and offset pointing capabilities; a separate artificial satellite ranging facility is located nearby (*12*). The station's 10-Hz repetition rate Nd-YAG laser produces 700 mJ per pulse at 1.064 mm. The yield on frequency doubling is half of this energy at 0.532 μm—the rest remains in the infrared (IR) spectrum. The pulse length is 350 ps, giving a transmitted pulse length of approximately 0.1 m. Technological innovations and upgrades at the Grasse station include experimental simultaneous ranging in the green and IR spectra and the use of high-speed and high-quantum efficiency photodiodes (instead of photomultipliers) for detectors. During the past 5 years, this dedicated station has produced the bulk of lunar ranging data, with 2- to 3-cm accuracy. Lunar laser ranging has also been occasionally carried out from (primarily) artificial satellite stations in Australia and Germany and has been proposed at several other stations around the world. Data from a global network of stations (Table 1) are clearly needed for a robust analysis program because the separation of parameters is enhanced by a geographically distributed network of observing sites.

The data set considered here consists of over 8300 normal-point ranges (*8*) spanning the period between August 1969 and December 1993; the observatories and the lunar reflectors included in the analysis are listed in Table 1. The data are analyzed with a model that calculates the light travel time between the observatory and the reflector, accounting for the orientation of the Earth and moon, the distance between the centers of the two bodies, solid tides on both bodies, plate motion, atmospheric delay, and relativity (*13*). The fitted parameters include the geocentric locations of the observatories; corrections to the variation of latitude (that is, polar motion); the orbit of the moon about the Earth; the Earth's obliquity, precession, and nutation; plus lunar parameters including the selenocentric reflector coordinates, fractional moment-of-inertia differences, gravitational third-degree harmonics, a lunar Love number, and rotational dissipation.

Orbits and Ephemeris Development

The computation of the round-trip light travel time between the ranging observatory and the lunar reflector depends on the geocentric location of the observatory, $\mathbf{R}_E$, the selenocentric position of the reflector, $\mathbf{R}_M$, and the distance between the centers of the Earth and moon, $\mathbf{r}$. For data analysis, the light time calculation is done with higher accuracy, but for purposes of discussion the approximate range (Fig. 3) is

$$\rho \simeq |\mathbf{r}| + \mathbf{R}_M \cdot \hat{\mathbf{r}} - \mathbf{R}_E \cdot \hat{\mathbf{r}} \qquad (1)$$

The mean Earth-moon distance is 385,000 km; the radii of the Earth and moon are 6371 and 1738 km, respectively.

The moon's orbit is strongly distorted from a simple elliptical path by the solar attraction—the instantaneous eccentricity varies by a factor of 2 (0.03 to 0.07). The perturbed orbit contributes a rich spectrum of range signatures that give sensitivity to a wide variety of parameters. The complications of the orbit are handled by simultaneous numerical integration of the orbits of the moon and nine planets (the lunar and planetary ephemeris) with the lunar rotation (lunar librations) (*14*). Although we used Cartesian coordinates rather than orbital elements as explicit parameters in our numerical integrations, analytical theories fit to the integrations provide information on the behavior of the orbital elements (*15*). The accuracy of the resulting ephemeris is set by the accuracy of the model for accelerations and the accuracy of the fit of the range data. The lunar ephemeris relies entirely on LLR data. The existing acceleration model accounts for relativistic forces between the sun, Earth, moon, and planets; gravitational harmonics of the Earth and moon; the orientation of the Earth's equator; the rotation of the triaxial moon (physical librations); tides, including tidal dissipation of energy on both the Earth and moon; and gravitational forces from the larger asteroids. The associated parameters such as masses, gravitational harmonic coefficients, and tidal strengths must be known a priori or must be included among the parameters fit in the least-squares solution to the time-delay measurements.

From the solution, the lunar orbit about the Earth is determined with great accuracy. Ranging data have provided a dramatic improvement compared to classical optical data in the accuracy of the lunar orbit. The orientation is determined at least two orders of magnitude more accurately, and the accuracy of the radial component is better by four orders of magnitude. The radial distance variations are determined better than the 2- to 3-cm range accuracy. The angular-rate uncertainty is no more than 0.3 ms of arc per year (*7*). The orbital components having the greatest uncertainties are the mean distance, presently 0.8 m due to correlation with the reflector coordinates in the mean-Earth direction, and the orientation of the orbit plane with respect to the Earth's equator, 1.5 ms of arc or 3 m at the lunar distance. These accuracies are degraded when extrapolated outside the span of observations. A continual supply of high-quality measurements and the accompanying analysis are required to maintain and enhance accuracies. The ephemerides are used for mission planning and spacecraft navigation.

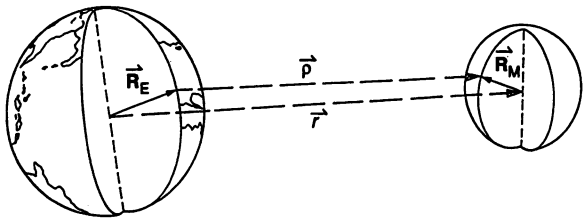

Fig. 3. The geometry of the Earth-moon system.

The strong influence of the sun on the lunar orbit permits the range data to be used to determine the mass ratio of the sun/(Earth + moon) and the relative orientation of the Earth-moon system orbit about the sun. The size of the Earth-moon orbit is set by the gravitational constant times the sum of the Earth's mass and the moon's mass, with the moon's orbit being deformed from a simple Keplerian ellipse by the influence of the sun. The two largest solar perturbations in distance $\mathbf{r}$ are 3699 km (monthly) and 2956 km (semimonthly). The few centimeter determination of the latter variation corresponds to 10^{-8} relative accuracy in the mass ratio (*16*). From fits, the mass ratio is found to be

$$\text{Mass}_{\text{sun}}/\text{Mass}_{(\text{Earth}+\text{moon})} = 328900.560 \pm 0.002 \qquad (2)$$

The solar perturbations allow the relative geocentric positions of the moon and sun to be determined to within 1 ms of arc. The planetary positions are known with respect to the Earth's orbit around the sun, so the geocentric position of the moon and the heliocentric positions of the planets can be made internally consistent in their relative orientation (*17*). Because the ranging stations are on the spinning Earth, the orientation of the equatorial plane is also determined relative to both the lunar orbit plane and the ecliptic plane of the heliocentric Earth-moon orbit. Thus, LLR is sensitive to the mutual orientation of the planes of the Earth's equator, the lunar orbit, and the ecliptic; hence, it locates the intersection of the ecliptic and equator planes (the dynamical equinox) and determines the angle between them (the obliquity of the ecliptic). The process of orienting the planetary ephemerides onto the fundamental astronomical reference frame is made possible at the millisecond-of-arc level with LLR data (*18*).

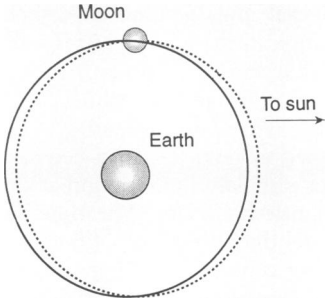

Fig. 4. Lunar orbit about the Earth as affected by the Nordtvedt term. A violation of the Equivalence Principle would cause the orbit of the moon about the Earth-moon center of mass to be polarized in the direction of the sun, with a characteristic size of ~13 m. The solid line represents the lunar orbit in General Relativity, and the dotted line represents the lunar orbit if the M_G/M_I values for the Earth and moon differ.

Gravitational Physics and Relativity

Lunar laser ranges, along with microwave ranges to planetary orbiting spacecraft and landers, have contributed strongly to solar system tests of gravitational theories. The moon and planets provide excellent test cases, because the ratio of nongravitational to gravitational forces acting on them is very small. For example, the ratio of the solar radiation pressure force on the moon to the gravitational attraction by the Earth is only 4×10^{-13}.

Shortly before the first Apollo landing, Nordtvedt (*19*) proposed a new test of general relativity that could be carried out using lunar range data. The Equivalence Principle, a fundamental tenet of General Relativity, states that the ratio of gravitational mass to inertial mass is the same for all bodies, independent of their composition (*20*). This principle had been tested in the laboratory but had not been tested for bodies large enough to have a significant fraction of their mass coming from gravitational self-energy. The Strong Equivalence Principle requires that all bodies fall with the same acceleration in an external gravitational field, with the gravitational self-energy contributing equally to the gravitational and inertial masses. Different metric theories of gravitation treat the interaction between gravity and gravitational energy differently; some predict violations of the Strong Equivalence Principle by massive bodies (*21*).

Since 1976, LLR data have been used to test the Strong Equivalence Principle (*22*). In magnitude, roughly 4.64×10^{-10} of the mass of the Earth is due to its gravitational self-energy, that is, the gravitational interaction energy of its different parts, while the corresponding fraction for the moon is much less (1.9×10^{-11}). With the moon orbiting the Earth, a violation of the Equivalence Principle would cause the orbit of the moon about the Earth-moon center of mass to be polarized in the direction of the sun (Fig. 4). This signature would have the synodic period of 29.53 days and is referred to as the Nordtvedt term. For a violation of the Strong Equivalence Principle, the ratio of the gravitational mass, M_G, to inertial mass, M_I, depends on the self-energy, U_G (*23, 24*)

$$M_G/M_I - 1 = \eta U_G/Mc^2 \quad (3)$$

where c is the speed of light and η is a parameter to be determined. Then the radial perturbation in the lunar orbit is

$$\delta r = C_0 \eta \cos D \quad (4)$$

where D is the angular elongation of the moon from the sun and $C_0 \sim 13$ m (*25*). Analysis with the early LLR data up to the mid-1970s confirmed General Relativity with $\eta = 0.00 \pm 0.03$ (*22*). Currently, LLR analyses give $(M_G/M_I - 1) = (2 \pm 5) \times 10^{-13}$, equivalent to $C_0\eta = -0.7 \pm 1.4$ cm or $\eta = -0.0005 \pm 0.0011$. The uncertainty in η assumes no violation of the Weak Equivalence Principle due to composition (*24, 26*). This is currently the best test of the Strong Equivalence Principle. Here, the errors are realistic rather than formal (*27*), with the uncertainty about a factor of 4 less than previously reported values (*28, 29*). With feasible improvements in the accuracy for lunar ranging and with continued data, further improvement is likely.

The above results can be interpreted as a test of the parameters β_R and γ_R from the Parametrized Post-Newtonian theory of gravitation, which in General Relativity have the values of $\beta_R = \gamma_R = 1$. The Nordtvedt coefficient, η, can be expressed as

$$4\beta_R - 3 - \gamma_R \quad (5)$$

The parameter β_R measures a superposition of gravitational effects and is commonly determined from the precession of perihelion for Mercury, while γ_R measures how much space curvature is produced by unit rest mass (*20*). Combining the above value for η with the result $\gamma_R = 1.000 \pm 0.002$ from analysis of the Viking lander tracking data (*30*) and assuming no violation of the Weak Equivalence Principle gives

$$\beta_R = 0.9999 \pm 0.0006 \quad (6)$$

The uncertainty is about a factor of 5 smaller than if β_R is derived from the precession of Mercury's perihelion (*29*).

A second important test of gravitational theory comes from the measurement of relativistic precession of the lunar orbit (termed geodetic precession), first predicted by de Sitter in 1916. According to General Relativity, this effect should cause a precession of the entire lunar orbit with respect to the inertial frame of the solar system by 19 ms of arc per year. The lunar range data are sensitive to this effect mainly through any excess precession of perigee beyond that due to the Newtonian effects of the sun, Earth, and other planets (*31*). The first observations of geodetic precession, in the late 1980s, agreed with the predictions of General Relativity to within their 2% accuracy (*32, 28*). New solutions presented here (Table 2) give a difference of $-0.3 \pm 0.9\%$ from the expected value. The error is partly due to an uncertainty in J_2, the primary lunar oblateness term (*33*).

Lunar range data also provide a test of a possible change in the gravitational constant (G) with time because of the lunar orbit sensitivity to solar longitude (*16*). Adding cosmological interest is the suggestion that quite large changes in G may have occurred during an inflationary phase in the early history of the universe [see, for example, (*34*)]. Estimates of limits from combining various types of solar system data including lunar data and Viking lander tracking data currently range from $|(dG/dt)/G| \leq 1 \times 10^{-11}$ to 0.4×10^{-11} per year (*35, 36*). The published limit from binary pulsar data is 2×10^{-11} per year (*37*). Our current uncertainty from analyzing lunar range data is similar to that reported by Chandler *et al.* (*35*).

Geodynamics

Lunar laser ranging measurements have permitted long-term studies of variations in the Earth's rotation, as well as the determination of constants of precession and nutation, station coordinates and motions, the Earth's gravitational coefficient, and tides accelerating the moon (*6, 7*). The more than two-decade-long span of LLR data exceeds that available from other space geodetic techniques. Lunar laser ranging has provided information about the exchange of angular momentum between the solid Earth and the atmosphere (*38*) and was instrumental in the discovery of the near 50-day oscillation in the length of day and its correlation with a similar oscillation in the atmosphere (*39*), which has stimulated research in the atmospheric community (*40*). Tidally driven periodic terms in Earth rotation have been studied and have been used to determine the response of the Earth (dependent on the Earth's structure and tides) at the fortnightly and monthly periods (*41*). The development of regular very long baseline interferometry (VLBI) measurement programs during the 1980s and refinement of satellite laser ranging programs have strongly complemented LLR results, providing more frequent and regular measurements in recent years (*38*).

The accurate value of the mass ratio of the sun/(Earth + moon) from LLR can be combined with the solar GM and the lunar GM from lunar-orbiting spacecraft (*42*) to

give the Earth's GM in an Earth-centered reference frame with accuracy of one part in 10^8 (see Table 2). Within the errors, this value is compatible with the value derived from ranges to artificial Earth satellites (*43*).

Tidal dissipation causes a misalignment of the tidal bulge of the Earth relative to the Earth-moon direction. The bulge exerts a secular torque, causing both the lunar orbit to expand as its angular momentum increases and the Earth's rotation rate to decrease. Most of the effect comes from the ocean tides, but a small unknown contribution comes from the mantle. The importance of the tidal acceleration of the moon is that it is the dominant cause of the long-term slowing of the Earth's rotation rate (other contributors are the tidal interaction with the sun and the change in the Earth's oblateness). The resulting change in the length of day has been seen in the geological record in a few special circumstances (*44*).

Because the lunar orbit is neither circular nor coplanar with the Earth's equator, the tides can be separated into distinct frequency components within bands near 0, 1, and 2 cycles per day. The tidally induced secular acceleration $\dot{n}$ of the lunar mean longitude is due mainly to the semidiurnal tides, with smaller contributions from the diurnal tides. The span and accuracy of the data are now sufficient to resolve the diurnal and semidiurnal contributions from the amplitude of the 18.6-year, along-track tidal perturbations (*45, 46*). The diurnal contribution is -4.04 ± 0.4 arcsec per century^2; the semidiurnal tides contribute -22.4 ± 0.6 arcsec per century^2 for a total of -26.28 ± 0.5 arcsec per century^2 (*46*). The small dissipation in the long-period tides is not modeled and is effectively included in the other components. This LLR-derived secular acceleration is compatible with those inferred from artificial satellite measurements of ocean tides (*47*) for both the diurnal and semidiurnal components. Dissipation in the moon itself is well established, but the contribution to the secular acceleration depends on which of two possible mechanisms of dissipation dominates: solid friction modeled by a constant time delay or turbulent fluid friction at the lunar core-mantle boundary. The time-delay lunar model that is used (*48, 49*) causes +0.4 arcsec per century^2, yielding a total secular acceleration of -25.88 ± 0.5 arcsec per century^2. If the dissipation is due to fluid friction at a core-mantle interface (*46*), the lunar contribution could be considerably smaller. The total tidal secular acceleration corresponds to an increase in the semimajor axis of 3.82 ± 0.07 cm/year.

Because of torques from the sun and moon, the Earth's spin axis precesses and nutates in space. These motions, designated luni-solar precession and nutation, respectively, depend on the flattening of the Earth [more specifically, the moment-of-inertia function (C − A)/C], the flattening of the core-mantle interface, and the Earth's anelasticity and ocean tides. Both LLR and VLBI analyses (*7, 50, 51*) have indicated that significant corrections are required to the standard precession and nutation model, as a consequence of geophysical effects. The nearly quarter-century span of the LLR observations is an advantage when trying to detect and separate the precession and 18.6-year nutation corrections; LLR analysis indicates that the correction to the standard precession constant is -3.3 ± 0.4 ms of arc per year (*7*), giving the luni-solar precession constant as 50.3845 s of arc per year. Further, the amplitude of the 18.6-year nutation in-phase term of the pole requires a correction of about 3 ms of arc, the magnitude of the term being increased, with a smaller out-of-phase term. Also detected was an annual correction of 2 ms of arc (*7, 50, 51*), which has been interpreted as being due to a 5% deviation in the flattening of the core-mantle boundary from that expected from hydrostatic equilibrium (*52*). An analogous discrepancy between theory and observation has been observed in tidal gravity data (*53*), with results consistent with this increased flattening of 5%. Joint solutions for precession and nutation have been made using LLR and VLBI data together, which combine the strength of the LLR data for the long time scale with the high resolution of the VLBI data for shorter periods (*54*).

Table 2. LLR determination of parameters.

Parameter	Value
Gravitational physics and relativity parameters	
Nordvedt effect	
$M_G/M_I - 1$	$(2 \pm 5) \times 10^{-13}$
η	-0.0005 ± 0.0011
$C_0\eta$	-0.7 ± 1.4 cm
Parametrized Post-Newtonian (PPN) parameter β_R	0.9999 ± 0.0006
Deviation from the expected geodetic precession	$-0.3 \pm 0.9\%$
Geophysical parameters	
GM_{EARTH}	$398{,}600.443 \pm 0.004$ km^3/s^2
Luni-solar precession constant at year 2000	50.3845 ± 0.0004 arcsec/year
18.6-year nutation corrections	
In-phase terms	
$\Delta\epsilon$	2.8 ± 1.1 marcsec
$\sin\epsilon\,\Delta\psi$	-2.9 ± 1.4 marcsec
Out-of-phase terms	
$\Delta\epsilon$	0.6 ± 1.3 marcsec
$\sin\epsilon\,\Delta\psi$	0.5 ± 1.0 marcsec
$\dot{n}$ secular acceleration of the moon	
Total	-25.88 ± 0.5 arcsec/century^2
Diurnal term	-4.04 ± 0.4 arcsec/century^2
Semidiurnal term	-22.24 ± 0.6 arcsec/century^2
Lunar contribution	+0.40 arcsec/century^2
Increase semimajor axis rate	3.82 ± 0.07 cm/year
Lunar parameters	
Love number, k_2	0.0302 ± 0.0012
Normalized moment of inertia, C/MR^2	0.3940 ± 0.0019
Dissipation parameters	
Q	26.5 ± 1.0
k_2/Q	0.001136 ± 0.000016
Second-degree moment differences	
$\beta_L = (C - A)/B$	$631.72 \pm 0.15 \times 10^{-6}$
$\gamma_L = (B - A)/C$	$227.88 \pm 0.02 \times 10^{-6}$
Low-degree gravitational harmonics	
J_2	$204.0 \pm 1.0 \times 10^{-6}$
C_{22}	$22.50 \pm 0.11 \times 10^{-6}$
J_3	$8.66 \pm 0.16 \times 10^{-6}$
C_{31}	$32.4 \pm 2.4 \times 10^{-6}$
S_{31}	$4.67 \pm 0.73 \times 10^{-6}$
C_{32}	$4.869 \pm 0.025 \times 10^{-6}$
S_{32}	$1.696 \pm 0.009 \times 10^{-6}$
C_{33}	$1.73 \pm 0.05 \times 10^{-6}$
S_{33}	$-0.28 \pm 0.02 \times 10^{-6}$

Lunar Science

The analysis of the LLR data provides a wealth of information concerning the dynamics and structure of the moon. The selenocentric reflector coordinates, the moment of inertia combinations, $\beta_L = (C -$

$A)/B$ and $\gamma_L = (B - A)/C$ (where $A < B < C$), and the second- and third-degree gravitational harmonics are determined with high accuracy (see Table 2). The coordinates for the lunar reflectors and the ALSEP radio transmitters serve as fundamental control points for lunar cartography (55). The distances between the retroreflectors and the Earth change in part because of lunar rotation (physical librations) and tides. Values of the gravitational harmonics, the moments of inertia and their differences, the lunar Love number, k_2 (which measures the tidal change in the moments of inertia and gravity), and variations in the lunar physical librations are related to the moon's composition, mass distribution, and internal dynamics.

Presently, the most accurate estimate of the lunar moment of inertia is obtained from combining the determinations of moment of inertia differences, β_L and γ_L, from the LLR solution (see Table 2) and the lunar gravity field coefficients $J_2\{ = [C - (B + A)/2]/MR^2\}$ and $C_{22}[= (B - A)/4MR^2]$ obtained from analysis of lunar satellite Doppler data (56) and LLR. The resulting polar moment from this combination is $C = (0.3935 \pm 0.0011)MR^2$. The lunar mass distribution also perturbs the lunar orbit, producing secular precessions in the lunar node and perigee directions (57). The lunar mass distribution contributions are -0.17 arcsec per year to the node rate and -0.02 arcsec per year to the perigee rate; the former changes the monthly range signature in $\mathbf{R}_E \cdot \hat{\mathbf{r}}$ by 0.5 m per year.

An interpretation of the polar moment is shown in Fig. 5 in terms of a 60-km-thick lunar crust with density of 2.75 g/cm^3, a constant-density (ρ) lunar upper mantle, a lower mantle with contrast in $\Delta\rho$ relative to the upper mantle, and a variable-radius iron core with density of 7 g/cm^3. The maximum core size is in the range of 220 to 350 km. An increase in crustal density to 2.959 g/cm^3 raises the maximum core size to 400 km. Magnetometer estimates of core size are ambiguous. Russell *et al.* (58) find a core radius of 435 ± 15 km, while Wiskerchen and Sonnet (59) only claim an upper bound of 400 km. The seismic constraint is less confining (60) with $R_c < 500$ km.

Two other major types of information concerning the lunar interior can be obtained from lunar libration data. One is the apparent tidal distortion of the moon, and the other is the mean direction of the spin axis. However, there are complications involved in interpreting the results. Consider the influences on lunar orientation arising from (i) inelastic deformation of the mantle shape with amplitude proportional to the tidal Love number and phase determined by the solid friction Q, (ii) turbulent dissipation at the core-mantle boundary (CMB) for a fluid core, and (iii) CMB ellipticity $e_c = (a - c)/a$. The primary lunar contribution to orientation variations is dependent on the mean lunar argument of latitude F (orbital mean longitude minus the ascending node on the ecliptic). The primary latitude variations along the Earth-moon direction (p_1) due to these effects (48, 49, 61) are

$$p_1 = \left[86k_2 + 4.9\frac{x(1-x) - y^2}{(1-x)^2 + y^2}\left(\frac{R_c}{350\text{ km}}\right)^5\right]\sin F + \left[230k_2/Q + 4.9\frac{y}{(1-x)^2 + y^2}\left(\frac{R_c}{350\text{ km}}\right)^5\right]\cos F \quad (7)$$

where we have adopted a core density of 7 g/cm^3 and the units are seconds of arc. Here, a value for x of $e_c/0.0040$ is the CMB ellipticity multiplied by the ratio of the 18.6-year nodal precession period to the lunar orbit period (62), and y is the core frictional parameter to be discussed later.

The apparent Love number (Table 2) presently obtained from LLR analysis, 0.0302 ± 0.0012, comes from the coefficient of the sin F term in p_1, with the possible CMB ellipticity ignored. It is much larger than expected, on the basis of naïve extensions of lunar seismic velocity profiles derived from the Apollo mission. Goins *et al.* (63) and Nakamura (60) deduced similar seismic velocity profiles in the upper mantle and strikingly different profiles in the middle mantle and provided essentially no constraints below ~1000 km in depth. This lack of constraints is partially due to the front-side cluster of seismic stations, the sparsity of detectable far-side impacts, and the ~1000-km maximum depth of deep-focus moonquakes. If we simply extend the observed S- and P-wave velocities down to a nominal 350-km-radius core, we obtain the following model values for k_2: 0.0245 (63) and 0.0215 (60).

Figure 6 shows k_2 deduced from the Goins *et al.* (63) and Nakamura (60) models from different S-wave velocities (V_s) below 1000 km in depth (note that the lunar radius is 1738 km) and lunar core sizes of radius 300 and 400 km, respectively. The 400-km core radius corresponds to the largest possible lunar core consistent with moment of inertia and magnetic constraints. The core size, within the limits considered, has only a small effect on k_2 (64). On the other hand, if a low-velocity zone below 1000 km in depth is added to the Goins *et al.* model, then the observed k_2 would be consistent with V_s of about 3.0 km/s. The ~40% decrease in V_s from middle mantle values can be explained only as arising from considerable partial melt, a much higher fraction than observed in a similar zone within the Earth. Clearly, the situation is even more implausible if the starting point

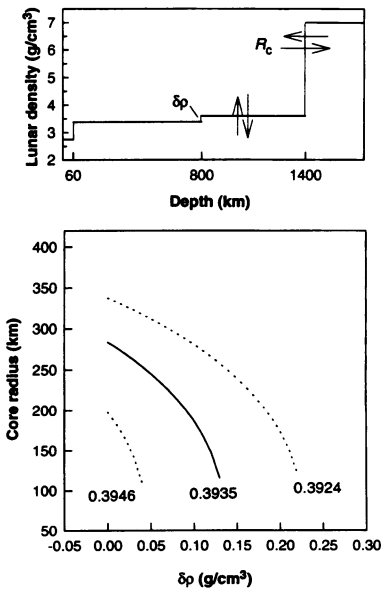

Fig. 5. Constraint on core radius from moment of inertia and lower mantle density contrast (δρ). For δρ, $R < 938$ km. The values for C/MR^2 are given below each trace in the bottom figure.

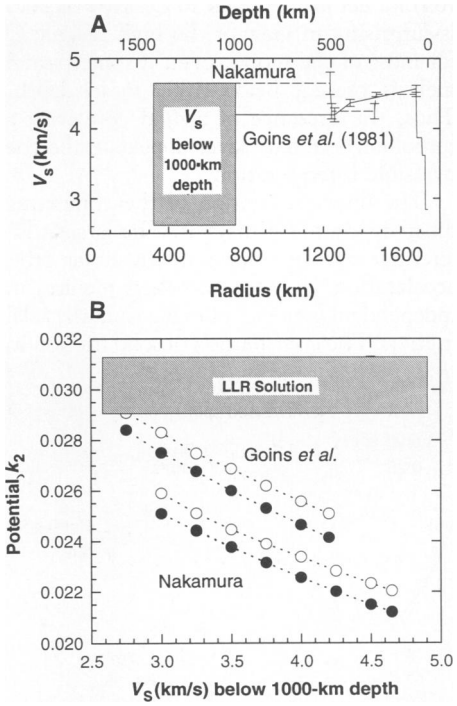

Fig. 6. (**A**) Love number (k_2) as a function of Apollo-derived shear wave velocity profiles (V_S) of Goins *et al.* (63) and Nakamura (60). (**B**) Comparison of LLR-determined value of k_2 made with that derived from variable V_S below 1000-km depths and core radius of 300 (filled circles) and 400 (hollow circles) km. Note that LLR value is independent of V_S. The range of V_S in (B) is represented by the shaded rectangle in (A).

is Nakamura's S-wave profile. Also, a large partial melt zone may face serious theoretical objections.

An alternative explanation for the apparent large k_2 value is the presence of a small core-boundary ellipticity $e_c = (a - c)/a$ that can partially mimic the k_2 libration signature, as can be seen from Eq. 7. The observed k_2 of 0.0302 (with $x = 0$) can be reduced to a value of 0.024 by the adoption of a core radius of 350 km and a core ellipticity, $a - c$, of $0.0004a$, or 140 m. Separation of the k_2 value from the core ellipticity effects depends on the detection of other periodic terms that are smaller. Therefore, a solution to this problem requires improvement in range accuracy.

If the moon were a perfectly rigid body, the mean direction of its spin axis would precess with the orbit plane. The lunar laser data show that the true spin axis of the moon is displaced from this expected direction by 0.26 arcsec (Fig. 7). The two dissipative terms proportional to cos F in Eq. 7 are due to solid and fluid dissipation. We can account for the observed 0.26-arcsec offset deduced from the lunar range by adopting either of the following: $k_2/Q = 0.001136 \pm 0.000016$ [or $Q \approx 26.5 \pm 1.0$ (Table 2)] or a value for the core frictional parameter of $y \cong 0.05$ (350 km/R_c)^5 [see (65) for details]. A value of Q as low as 26.5 is surprising in view of the high seismic Q for most of the moon, even if some partial melt is present below 1000 m in depth. Thus, the presence of a fluid core with a turbulent boundary layer appears to be the plausible interpretation.

The direct separation of the competing dissipative terms is difficult. The largest differential signature arises in the lunar orbit acceleration, and separation here requires an independent estimate of $\dot{n}$ due to Earth tidal friction. The contribution of solid friction in the moon to the secular $\dot{n}$ is 0.4 arcsec per century^2 (66), while that due to core surface, fluid friction is about a factor of 3 smaller. In principle, the difference in $\dot{n}$ could be detected by comparing the total $\dot{n}$ measured by LLR with $\dot{n}$ predicted from artificial satellite measurements of ocean tides (48). Unfortunately, the present determinations are not yet precise enough to discriminate between these two alternatives.

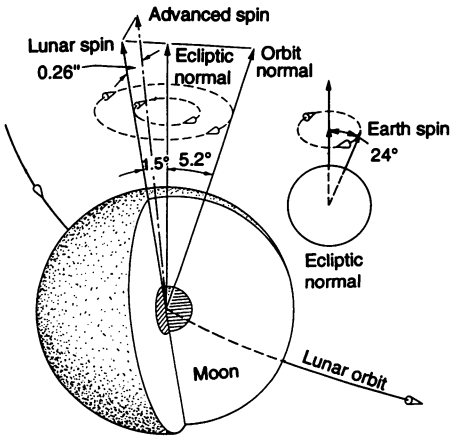

Fig. 7. Orientation of the moon relative to the Cassini state. The Cassini state has the ecliptic pole, orbit pole, and spin axis in the same plane. The latter two precess about the ecliptic pole with an 18.6-year period.

It also is worthwhile to mention the observation of an apparent free libration of the moon. Separate from librations driven by the time-varying torques of the Earth and sun (the forced physical librations), three modes of free libration exist. One of these rotational modes is analogous to the Earth's Chandler wobble (but with a 74-year period), another is an oscillation of the pole direction in space (in addition to the uniform precession), and the last is a 2.9-year oscillation in rotation speed (longitude). Without suitable recent exciting torques, and because of the substantial dissipation, the amplitudes of these free librations should have damped to zero. However, the LLR data show an apparent rotational free libration in longitude for the moon with 2.9-year period and amplitude of 1 arcsec (67).

There is uncertainty over this 2.9-year free libration, because some very small forcing term in the lunar orbit near the resonance frequency for the free libration may be amplified strongly to mimic the free motion. The numerically integrated rotational motions of the moon have been compared with semi-analytic calculations of the forced angular motions to separate out the free motion. However, the semi-analytic results may not be sufficiently accurate or complete to rule out the possibility that the observed motion is actually a forced motion.

Studies have been carried out to investigate whether the apparent free libration is likely to have been excited by impacts on the moon (68). Such excitation would have required an impact in very recent times by an object large enough to leave a crater with a 10-km diameter, statistically a highly unlikely event. Seismic events on the moon also cannot explain the observed amplitude. Passes through weak resonances have occurred in the geologically recent past and can stimulate free librations in longitude (69). A plausible explanation appears to be core boundary effects, similar to those that are believed to account for the decade-scale fluctuations in the Earth's rotation (48).

Future Prospects

The past quarter century has been a productive period for LLR, including several landmark results such as the verification of the Strong Equivalence Principle with unprecedented accuracy, orders-of-magnitude improvements in the determination of the lunar rotation (physical librations), the indication of a probable liquid lunar core, and the accurate determination of the lunar tidal acceleration and the Earth's precession. Lunar laser ranging is the only working experiment that continues the Apollo legacy, and because of its passive nature, it can continue as long as proper ground-based ranging stations are maintained.

Over the lifetime of the LLR experiment, the range accuracy has improved by an order of magnitude from 25-cm uncertainty in the early 1970s to today's 2- to 3-cm ranges. The precision on some days reaches 1 cm, but the calibration accuracy for the timing systems is not yet this good. The accuracy limitation due to the atmosphere appears likely to be only about 2 mm at a 45° elevation angle (70).

For the immediate future, we have under way the implementation of dramatically increased station computing power, offset guiding capability, and hands-off auto guiding. The benefits from the above applications will not only be an increased number of normal points spread over significantly more of the lunar phase but also a significantly increased number of photons within a given normal point. The more extended and denser lunar phase coverage means greater sensitivity to many of the lunar solution parameters. The increased number of photons per normal point will provide better operational precision and perhaps aid in improving the accuracy.

Farther down the road, we foresee the availability of more precise and more efficient photon detectors, such as micro-channel plates, significantly improved timing systems, and shorter pulse, more powerful lasers. These will provide higher accuracy, additional sensitivity to lunar parameter signatures, and a further increase in the lunar data density. On the more distant horizon, lunar missions have been proposed that could place microwave or optical transponders (71) at widely separated lunar sites. These devices would permit differential measurements with up to two orders of magnitude improvement in accuracy.

The expected increased data density and improved accuracy in the future will permit greater understanding of the Earth, the moon, and the Earth-moon system, answering old questions and revealing new phenomena to be explored. Advances in ephemeris development will continue, and improved tests of gravitational physics and relativity are expected.

REFERENCES AND NOTES

1. C. O. Alley *et al.*, *J. Geophys. Res.* **70**, 2267 (1965); C. O. Alley and P. L. Bender, *Proceedings of the International Astronomical Union Sympo-*

sium No. 32, Continental Drift, Secular Motion of the Pole, and Rotation of the Earth, W. Markowitz and B. Guinot, Eds. (Reidel, Dordrecht, Netherlands, 1968), pp. 86–90; C. O. Alley *et al.*, in *The Application of Modern Physics to the Earth and Planetary Interiors*, S. K. Runcorn, Ed. (Wiley-Interscience, New York, 1969), pp. 523–530; C. O. Alley *et al.*, *Science* **167**, 458 (1970); C. O. Alley, in *Adventures in Experimental Physics, 1*, B. Maglic, Ed. (World Science Communications, Princeton, NJ, 1972), pp. 127–156; C. O. Alley *et al.*, in *Apollo 11 Preliminary Science Report, NASA SP-214* (Clearing House for Federal Scientific and Technical Information, Springfield, VA, 1969), pp. 163–182.

2. J. G. Williams, in *Scientific Applications of Lunar Laser Ranging*, J. D. Mulholland, Ed. (Reidel, Dordrecht, Netherlands, 1977), pp. 37–50; P. L. Bender *et al.*, *Science* **182**, 229 (1973).
3. J. D. Mulholland, *Rev. Geophys. Space Phys.* **18**, 3 (1980); *ibid.*, p. 549.
4. C. O. Alley, in *Quantum Optics, Experimental Gravity, and Measurement Theory*, P. Meystre and M. O. Scully, Eds. (Plenum, New York, 1983), pp. 429–495.
5. J. O. Dickey, J. G. Williams, X X Newhall, *Proceedings of the Fifth International Workshop of Laser Ranging Instrumentation.* J. Gaignebet, Ed. (Royal Greenwich Observatory, Greenwich, UK, 1986), vol. 1, pp. 19–28.
6. A. L. Whipple, *Adv. Space Res.* **13** (no. 11), 213 (1993).
7. J. G. Williams, X X Newhall, J. O. Dickey, in *Contributions of Space Geodesy to Geodynamics: Earth Dynamics*, vol. 24 of *Geodynamics Series*, D. E. Smith and D. L. Turcotte, Eds. (American Geophysical Union, Washington, DC, 1993), pp. 83–88.
8. The LLR observing process is normally broken up into individual runs for particular lunar surface retroreflectors. Each of these runs is composed of 5 to 100 reflections distributed over 10 to 45 min of time. The number of individual observation events grows rapidly, and from the earliest days of the LLR experiment, data compression into normal points has been the rule. The complete LLR normal-point construction process is described by Abbot *et al.* [*Astron. J.* **78**, 784 (1973)].
9. J. Faller *et al.*, *Science* **166**, 99 (1969); C. O. Alley *et al.*, *ibid.* **167**, 368 (1970).
10. E. C. Silverberg, *Appl. Opt.* **13**, 565 (1974); R. I. Abbot *et al.*, *Astron. J.* **78**, 784 (1973); P. J. Shelus *et al.*, *ibid.* **80**, 154 (1975); J. D. Mulholland *et al.*, *ibid.*, p. 1087.
11. P. J. Shelus, *IEEE Trans. Geosci. Remote Sensing* **GE-234**, 385 (1985); ———, R. L. Ricklefs, A. L. Whipple, in *Contributions of Space Geodesy to Geodynamics: Technology*, vol. 25 of *Geodynamics Series*, D. E. Smith and D. L. Turcotte, Eds. (American Geophysical Union, Washington, DC, 1993), pp. 183–187.
12. C. Veillet *et al.*, in *Proceedings of the Seventh International Workshop on Laser Ranging Instrumentation*, C. Veillet, Ed. (Observatoire de la Côte d'Azur, Grasse, France, 1989), 149–156.
13. X X Newhall, J. G. Williams, J. O. Dickey, in *Proceedings of the International Association of Geodesy (IAG) Symposia* (Bureau Central de l'A.I.G., Paris, 1987), vol. 78, pp. 78–82.
14. X X Newhall, E. M. Standish, J. G. Williams, *Astron. Astrophys.* **125**, 150 (1983).
15. M. Chapront-Touze and J. Chapront, *ibid.* **124**, 50 (1983); *ibid.* **190**, 342 (1988); *Lunar Tables and Programs from 4000 B.C. to A.D. 8000* (Willmann-Bell, Richmond, VA, 1991).
16. The distance from the center of the Earth to the center of the moon can be represented by the series with largest terms (in kilometers)

$$385001 - 20905 \cos \ell - 3699 \cos (2D - \ell) - 2956 \cos 2D$$

The first term is the mean distance, the second results from the eccentricity of the orbit, and the third and fourth are solar perturbations. The lunar mean anomaly is ℓ, and D is the mean elongation of the moon from the sun. Determination of the mean distance and the lunar period of the second term would give gravitational mass of the Earth-moon system or its mass ratio with the sun, but the coordinate of the retroreflectors in the Earth's mean direction mimics the mean distance. The amplitude of the fourth term depends on the mean distance and the monthly and annual orbital periods. The period of D in the third and fourth terms depends on the annual period. Consequently, the mass ratio and gravitational mass can be determined from the amplitude of the fourth term and the periods of the last three terms. In this article, analytical equations like the above are used for discussions; the actual analysis uses numerical partial derivatives.
17. J. G. Williams and E. M. Standish, in *Reference Frames in Astronomy and Geophysics*, J. Kovalevsky, I. I. Mueller, B. Kolaczek, Eds. (Kluwer Academic, Dordrecht, Netherlands, 1989), pp. 67–90.
18. Consider the component of range

$$\mathbf{R_E} \cdot \hat{\imath} \approx R_Z \sin \delta + R_S \cos \delta \cos H$$

where $\sin \delta \approx \sin \varepsilon \sin \lambda + \sin i \sin u$, R_Z and R_S are the polar and equatorial components of the station vectors (Fig. 3), respectively, and H is the local hour angle of the reflector. The declination (δ) depends on the obliquity (ϵ), lunar longitude measured from the equinox (λ), lunar orbit inclination (i), and angle between the moon and its node on the ecliptic (u). Consequently, sensitivity to these quantities comes from the projection of the station vector along the Earth-moon direction.
19. K. Nordtvedt, *Phys. Rev.* **170**, 1186 (1968).
20. C. M. Will, *Theory and Experiment in Gravitational Physics* (Cambridge Univ. Press, Cambridge, 1981).
21. For example, see C. Brans and R. H. Dicke, *Phys. Rev.* **124**, 925 (1961).
22. I. I. Shapiro, C. C. Counselman III, R. W. King, *Phys. Rev. Lett.* **36**, 555 (1976); J. G. Williams *et al.*, *ibid.*, p. 551.
23. The gravitational self-energy of the body, U_G, is

$$-\frac{G}{2}\int \frac{\rho(\mathbf{x})\,\rho(\mathbf{x}')\,dV\,dV'}{|\mathbf{x}-\mathbf{x}'|}$$

where $\rho(x)$ is the density, $\mathbf{x}$ is the position vector, and V indicates volume. The value of U_G/Mc^2 for the Earth equals -4.64×10^{-10}, while for the moon, it is -0.19×10^{-10}. The difference between Earth and moon for U_G/Mc^2 and M_G/M_I enters Eq. 3. The partial derivative for M_G/M_I is derived from numerical integrations.
24. K. Nordtvedt, *Phys. Rev. D* **37**, 1070 (1988).
25. ———, unpublished results.
26. E. G. Adelberger, B. R. Heckel, G. Smith, Y. Su, H. E. Swanson, *Nature* **347**, 261 (1990).
27. To achieve what are usually called realistic errors, solutions involving a number of different subsets of the data and of the parameters have been carried out to investigate the stability of the results. In addition, for the error of the coefficient of cos D, a hypothetical 1-cm uncertainty has been included that is equivalent to 3.5×10^{-13} in M_G/M_I.
28. J. O. Dickey, X X Newhall, J. G. Williams, *Adv. Space Res.* **9** (no. 9), 75 (1989).
29. I. I. Shapiro, in *General Relativity and Gravitation*, N. Ashby, D. F. Bartlett, W. Wyss, Eds. (Cambridge Univ. Press, Cambridge, 1990), p. 313.
30. R. D. Reasenberg *et al.*, *Astrophys. J. Lett.* **234**, L219 (1979).
31. B. Bertotti, I. Ciufolini, P. L. Bender, *Phys. Rev. Lett.* **58**, 1062 (1987).
32. I. I. Shapiro *et al.*, *ibid.* **61**, 2643 (1988).
33. The lunar J_2 uncertainty dominates, contributing 0.6% to the error.
34. D. La and P. J. Steinhardt, *Phys. Rev. Lett.* **62**, 376 (1989).
35. J. F. Chandler, R. D. Reasenberg, I. I. Shapiro, *Bull. Am. Astron. Soc.* **25**, 1233 (1993).
36. R. W. Hellings *et al.*, *Phys. Rev. Lett.* **51**, 1609 (1983).
37. T. Damour, G. W. Gibbons, J. H. Taylor, *ibid.* **61**, 1151 (1988); J. H. Taylor and J. M. Weisberg, *Astrophys. J.* **345**, 434 (1989). The limit of the latter paper has been increased for coupled mass and angular momentum changes [see K. Nordtvedt, *Phys. Rev. Lett.* **65**, 953 (1990)].
38. R. Hide and J. O. Dickey, *Science* **253**, 629 (1991), and references therein.
39. M. Feissel and D. C. Gambis, *C. R. Acad. Sci. Paris* **B291**, 271 (1980); R. B. Langley *et al.*, *Nature* **294**, 730 (1981).
40. J. D. Anderson and R. D. Rosen, *J. Atmos. Sci.* **40**, 1584 (1983); R. A. Madden. *J. Geophys. Res.* **93**, 5333 (1988); *ibid.* **92**, 8391 (1987); J. O. Dickey, M. Ghil, S. L. Marcus, *ibid.* **96**, 22643 (1991); M. Ghil and K. Mo, *J. Atmos. Sci.* **48**, 752 (1991).
41. C. F. Yoder, J. G. Williams, M. E. Parke, *J. Geophys. Res.* **86**, 881 (1981).
42. A. J. Ferrari *et al.*, *ibid.* **85**, 3939 (1980).
43. J. C. Ries, R. J. Eanes, C. K. Shum, M. M. Watkins, *Geophys. Res. Lett.* **19**, 529 (1992).
44. K. Lambeck, *The Slow Deformation of the Earth, Geophysical Geodesy* (Clarendon Press, Oxford, 1988).
45. J. G. Williams, W. S. Sinclair, C. F. Yoder, *Geophys. Res. Lett.* **5**, 943 (1978).
46. J. G. Williams, X X Newhall, J. O. Dickey, *Eos* **73** (no. 43), 126 (1992).
47. J. G. Marsh *et al.*, *J. Geophys. Res.* **95**, 22043 (1990); M. K. Cheng, R. J. Eanes, B. D. Tapley, *Geophys. J. Inter.* **108**, 401 (1992).
48. C. F. Yoder, *Philos. Trans. R. Soc. London Ser. A* **303**, 327 (1981).
49. ———, in *Natural and Artificial Satellites*, P. E. Nacozy and S. Ferraz-Mello, Eds. (Univ. of Texas Press, Austin, 1979), pp. 211–221.
50. J. G. Williams, X X Newhall, J. O. Dickey, *Astron. Astrophys.* **241**, L9 (1991).
51. T. A. Herring *et al.*, *J. Geophys. Res.* **91**, 4745 (1986); W. E. Himwich and E. J. Harder, in *The Earth's Rotation and Reference Frames for Geodesy and Geodynamics*, A. K. Babcock and G. A. Wilkins, Eds. (Kluwer, Dordrecht, Netherlands, 1988), pp. 301–307; S. Y. Zhu *et al.*, *Astron. J.* **99**, 1024 (1990); J. A. Steppe, S. O. Oliveau, O. J. Sovers, *IERS Technical Report No. 5*, M. Feissel, Ed. (Observatoire de Paris, Paris, 1990), pp. 13–24; T. A. Herring *et al.*, *J. Geophys. Res.* **96**, 8259 (1991).
52. C. R. Gwinn, T. A. Herring, I. I. Shapiro, *J. Geophys. Res.* **91**, 4755 (1986).
53. J. Hinderer, D. Jault, H. Legros, J.-L. Le Mouël, *Phys. Earth Planet. Inter.* **59**, 329 (1990).
54. P. Charlot, O. J. Sovers, J. G. Williams, X X Newhall, *Proceedings of the 127th Colloquium of the International Astronomical Union, Reference Systems*, C. A. Smith, and G. H. Kaplan, Eds. (U.S. Naval Observatory, Washington, DC, 1991), vol. 228.
55. J. G. Williams, X X Newhall, J. O. Dickey, *Lunar Gravitational Harmonics and Reflector Coordinates, Proceedings of the International Symposium: Figure and Dynamics of the Earth, Moon and Planets*, special issue of the *Monograph Series of the Research Institute of Geodesy, Topography and Cartography*, P. Holota, Ed. (Research Institute of Geodesy, Topography and Cartography, Prague, 1987), pp. 643–648; R. W. King, C. C. Counselmann III, I. I. Shapiro, *J. Geophys. Res.* **81**, 6251 (1976); M. E. Davies, T. R. Colvin, D. L. Meyer, *ibid.* **92**, 14177 (1987).
56. A. S. Konopliv, W. L. Sjogren, R. N. Wimberly, R. A. Cook, A. Vijayaraghavan, AAS 93-622 at *Proceedings of the American Astronautical Society–American Institute for Aeronautics and Astronautics Astrodynamics Specialist Conference*, Victoria, Canada, 16 to 19 August 1993 (Unibelt, San Diego, CA, 1993). The gravity coefficients measure the distortion from a spherical field. The lunar J_2 describes an equatorial bulge, and C_{22} describes a bulge along the mean Earth-moon direction. They obtain $J_2 = 203.8 \times 10^{-6}$ and $C_{22} = 22.37 \times 10^{-6}$. For weak coupling to the core, the inferred moment should be decreased by a factor of $(1 - C_c/C)$.
57. W. J. Eckert, *Astron. J.* **70**, 787 (1965); N. Borderies and C. F. Yoder, *Astron. Astrophys.* **233**, 235 (1990). The nodal contribution is $-(3/2)n(R/a)^2 \sin (I + \epsilon)/\sin I\,(J_2 + 2C_{22}) = -0.17$ arcsec per year,

where n is the mean motion, R/a the ratio of lunar radius to semi-major axis, ϵ the obliquity, and I the orbital inclination.
58. C. T. Russell, P. J. Coleman Jr., B. E. Goldstein, *Proc. Lunar Planet. Sci. Conf.* **128**, 831 (1981).
59. M. J. Wiskerchen and C. P. Sonnett, *ibid.* **1**, 515 (1977).
60. Y. Nakamura, *J. Geophys. Res.* **88**, 677 (1983).
61. D. H. Eckhardt, *Moon Planets* **25**, 3 (1981).
62. The value of x is
$$\frac{(a-c)}{a}\left(\frac{18.6\text{ years}}{27.3\text{ days}}\right)=\frac{e_c}{0.0040}$$
63. N. R. Goins, N. M. Toksöz, A. M. Dainty, *Proc. Lunar Planet. Sci. Conf.* **3**, 2424 (1979); N. R. Goins, A. M. Dainty, M. N. Toksöz, *J. Geophys. Res.* **86**, 5061 (1981).
64. The value of Δk is k_2 (400 km) − k_2 (300 km) ≃ 0.001.
65. The core frictional parameter y is related to the friction coupling parameter K by
$$y = K\left(\frac{18.6\text{ years}}{27.3\text{ days}}\right)=\frac{K}{0.0040}$$
where the frictional torque is $KI_c\,\omega\,(\omega-\omega_c)$ and ω and ω_c are the angular velocity vectors of mantle and core, respectively. For turbulent skin friction, K is $(45\pi/32)\kappa$ sin $\Delta\epsilon$. Here, $\Delta\epsilon$ is the differential obliquity of core and mantle spin vectors and is approximately equal to mantle obliquity (1.54°) for weak frictional and Poincaré pressure coupling. In turn, the local skin friction parameter κ can be derived through simple flat plate theory and is on the order of 0.001 to within a factor of 2. A 350-km core radius (with core density = 7 g/cm^3) corresponds to κ = 0.0016.
66. The contribution of solid friction in the moon to the secular dn/dt is
$$\frac{dn}{dt}\approx\frac{9}{2}\frac{k_2}{Q}\frac{M_{Earth}}{M_{moon}}\left(\frac{R}{a}\right)^5 n^2[7e^2+\sin^2(I+\epsilon)] =$$
0.4 arcsec per century^2
where e is the orbital eccentricity.
67. O. Calame, in (*2*), pp. 53–63; R. J. Cappallo, R. W. King, C. C. Counselman III, I. I. Shapiro, *Celestial Mech.* **26**, 145 (1982); J. G. Williams, X X Newhall, J. O. Dickey, *Eos* **72** (no. 17), 179 (1991).
68. S. J. Peale, *J. Geophys. Res.* **81**, 1813 (1976).
69. D. H. Eckhardt, *Celestial Mech. Dyn. Astron.* **57**, 307 (1993).
70. P. L. Bender, in *Refraction of Transatmospheric Signals in Geodesy*, J. C. De Munck and T. A. Th. Spoelstra, Eds. (Netherlands Geodetic Commission no. 36, Delft, 1992), pp. 117–125; T. A. Herring, *ibid.*, pp. 157–164. The total atmospheric correction uncertainty given by Bender in Case II of Table 1 is 2 mm at 45° elevation, with one of the two largest contributions being from uncertainties in horizontal gradients. The horizontal gradient effect assumed for Case II is just equal to the total tropospheric horizontal gradient effect for radio waves found by Herring from extensive VLBI measurements. The horizontal gradient contribution should be smaller for laser propagation than for radio waves.
71. P. L. Bender *et al.*, *Astrophysics from the Moon, AIP Conference Proceedings 207*, M. J. Mumma, H. J. Smith, G. H. Linebaugh, Eds. (American Institute of Physics, New York, 1990), pp. 647–653.
72. It is impossible to acknowledge all who have been responsible for the achievements described here. The original NASA LURE Team must be listed (in alphabetical order): C. O. Alley, P. L. Bender, D. G. Currie, R. H. Dicke, J. E. Faller, W. M. Kaula, J. D. Mulholland, H. H. Plotkin, E. C. Silverberg, and D. T. Wilkinson. We acknowledge and thank E. C. Silverberg for his pioneering efforts at McDonald Observatory in the early years of the LLR experiment. The success of the early program would not have been possible without the strong support of the late H. J. Smith. We also acknowledge the staffs at CERGA, Haleakala, and McDonald Observatory. We are grateful to K. Nordtvedt and T. Damour for comments that improved the manuscript. Normal points were constructed from individual photon returns by R. Ricklefs, P. Shelus, A. Whipple, and J. G. Ries at the University of Texas at Austin for the MLRS and for earlier Haleakala data. D. O'Gara produced later Haleakala normal points. C. Veillet provided normal points for the CERGA data. The work of four of the authors (J.O.D., XXN., C.F.Y., and J.G.W.) presents the results of one phase of research carried out at the Jet Propulsion Laboratory, California Institute of Technology, under contract with the National Aeronautics and Space Administration (NASA). The University of Texas authors (R.L.R., J.G.R., P.J.S., A.L.W., and J.R.W.) acknowledge support from NASA and the U.S. Naval Observatory.

Mobile Point Defects and Atomic Basis for Structural Transformations of a Crystal Surface

Ing-Shouh Hwang,* Silva K. Theiss, J. A. Golovchenko†

Structural transformations on elemental semiconductor surfaces typically occur above several hundred degrees Celsius, and the atomic motions involved are extremely rapid and difficult to observe. However, on the (111) surface of germanium, a few lead atoms catalyze atomic motions so that they can be observed with a tunneling microscope at temperatures below 80°C. Mass transport and structural changes are caused by the creation and propagation of both vacancy-like and interstitial-like point defects within the crystal surface. The availability of dangling bonds on the surface is critical. A detailed atomic model for the observed motions has been developed and is used to explain the structural phase transition Ge(111)-c(2×8) ↔ 1×1, which occurs near 300°C.

Interest in diffusion and phase transitions can be said to date back to the earliest days of metallurgy. That interest continues unabated today because our ability to create complex materials with useful properties and the stability of these materials depend on these phenomena. Both diffusion and structural transformations proceed through mechanisms that operate on the atomic scale, and fundamental understanding has come from indirect methods and reasoning. In single crystals, bulk diffusion is effected primarily by the motion of point defects: vacancies and interstitial atoms (*1*, *2*). A vacancy can move from one substitutional site in a lattice to another and thus lead to mass transport in the opposite direction. An interstitial atom may either diffuse through the lattice until it combines with a vacancy (the interstitial mechanism), or it may replace a substitutional atom, displacing that atom into an adjacent interstitial site (the interstitialcy or kick-out mechanism). Diffusion that is constrained entirely within a single plane of atoms at a surface may be viewed as the two-dimensional analog of bulk diffusion. It likewise requires mobile point defects. Unlike the bulk, however, the surface is accessible to direct, atomic-scale study. In addition, improved understanding of surface dynamics is of importance in its own right and would benefit disciplines extending from chemistry to electronics.

In recent years, there has been growing interest in the use of the scanning tunneling microscope (STM) for real time and space observations of the fundamental mechanisms of surface mass transport (*3*–*8*). One of the main problems in such a study is the slow scanning speed of the current generation of tunneling microscopes, which often cannot follow atomic motions occurring on crystal surfaces. A possible solution is to design STMs that can somehow take images more quickly. Another is to find a way to catalyze the atomic motions such that they occur at lower temperatures, where atomic motions are slower and can be clearly identified by the STM. Such catalysis could be of great practical use as well, for example, in crystal growth.

A small number of impurity Pb atoms on a Ge surface catalyze atomic motions and structural changes without altering the basic mechanisms involved. The present study evolved from our work on Pb atom diffusion, which involves interchanges of individual Pb atoms with Ge adatoms (*4*). The diffusion tends to occur along the Ge

I.-S. Hwang is with the Division of Applied Sciences, Harvard University, Cambridge, MA 02138, USA. S. K. Theiss is with the Department of Physics, Harvard University, Cambridge, MA 02138, USA. J. A. Golovchenko is with the Department of Physics and Division of Applied Sciences, Harvard University, Cambridge, MA 02138, and Rowland Institute for Science, Cambridge, MA 02142, USA.

*Present address: Institute of Physics, Academia Sinica, Taipei, Taiwan, Republic of China.
†To whom correspondence should be addressed.